EXPERIMENTAL STUDY OF THE INFLUENCE OF SURFACE NON-CONFORMANCES ON THE LOW PRESSURE TURBINE OUTLET GUIDE VANE FLOW

Harshad Lalit*, Valery Chernoray*, Jonas Larsson**

*** Department of Applied Mechanics, Chalmers University of Technology**
412 96 Gothenburg, Sweden
**** Department of Aero and Thermo Dynamics, Volvo Aero Corporation**
461 81 Trollhättan, Sweden

Keywords: *guide vane, wall protuberance, losses, flow separation, turbulence modelling*

Abstract

During manufacturing and in-service of the outlet guide vanes various irregularities on the vane surface can occur. These irregular shapes are surface non-conformances in the form of welds, traces or repairs of various forms. Improvement of the aerodynamic performance of the guide vanes requires understanding of the impact of these technological features on the flow field and aerodynamics.

Experimental study is performed in a linear cascade facility at Chalmers University. In focus of current work are non-conformances in form of welding traces. The model welding traces were placed at different locations on the suction side of the vane. The influence of these non-conformances on the cascade aerodynamics is evaluated and validation of CFD results obtained by the k-ε realizable and k-ω SST turbulence models is performed.

1 Introduction

Low pressure turbine outlet guide vanes (LPT OGVs) are positioned in the last vane row in a low pressure turbine. The OGVs have both an aerodynamic and a structural function. In structural terms they compose a frame which provides a structural connection between the aft bearing support, the main engine carcass and the aircraft attachment point. In aerodynamic terms they form the last part of the engine internal flow path before the nozzle. The main aerodynamic function of the OGVs is to de-swirl the flow coming from the last low-pressure turbine rotor, into an axial outflow. Both the high structural loads and the relatively large support lines passing through the OGVs make them thick and hence challenging to optimize in terms of aerodynamic losses and flow separation. The turning flow and area change result in a diffusing flow with growing boundary layers, strong secondary flows, and high risk of separation. The swirl angle upstream of the OGVs typically varies between ±10 degrees from design conditions, and the off-design requirements dictate the absence of the flow separation at the vane mid-span.

The problem of surface non-conformances is of high importance for OGVs. The OGV manufacturing and in-service may lead to different defects on the vane surface such as welds or surface repair patches. Because of being highly three-dimensional surfaces the manufacturing process of the OGVs is difficult to maintain under the tight tolerances imposed. Furthermore, the OGVs are typically not replaced during the engine service and subjected to a long time of erosion, potential damages and repairs during the whole engine lifetime.

The efficiency of the low-pressure turbine has a significant effect of the overall specific

fuel consumption of an aero-engine. A 1% increase in LPT efficiency gives rise to 0.7% increase in overall engine efficiency [1]. Therefore increasing the engine efficiency requires knowledge of the implication of the manufacturing inaccuracies on the aerodynamic performance of the OGVs.

It appears that some production and in-service defects of the OGVs can influence boundary layers, transition and losses significantly, while other can be considered as insignificant and tolerated without an additional expensive machining. It is also vital to know which damages may need a replacement and which can be repaired. An ideal location of such a repair or manufacturing defect can also be determined to have the minimal impact on the OGV aerodynamics. Of particular importance for the aerodynamic optimization is to have reliable and validated CFD design tools, which means that high-quality experiments are necessary for validation. A literature survey doesn't show any publicly available studies of same type and therefore the current study was initiated.

2 Experimental Setup

Experiments were performed in Chalmers linear cascade facility which is of open circuit blower type. The OGV cascade has 7 vanes, see Fig.1. The cross section of the working part of the facility is 200 by 1200 mm. The flow is driven by a 30 kW centrifugal fan and passes trough a wide-angle diffuser, a settling chamber, and a contraction. The test section is equipped with an end wall boundary layer suction system. The design and validation of the facility is described in detail by Hjärne et al. [2,3] and Hjärne [4]. The facility is operated at Reynolds number of 300,000 based on the vane chord, which is typical for OGV flows. In current study the flow incidence angle was kept at a constant value of 30 degrees and the incoming velocity was adjusted to be around 20 m/s. The level of the incoming flow turbulence intensity was adjusted by a turbulence grid which was placed 700 mm upstream of the cascade and parallel to the cascade leading edge plane, see Fig. 1.

Cascade vanes are manufactured using a stereo lithography technique which has a typical accuracy of ±0.1 % of the model size. Models produced by this method have small traces on the surface due to a finite resolution of the machine. These traces were filled with putty and thereafter the vanes were polished. The level of the surface deviations present in the baseline geometry was additionally controlled by a 3D scanner.

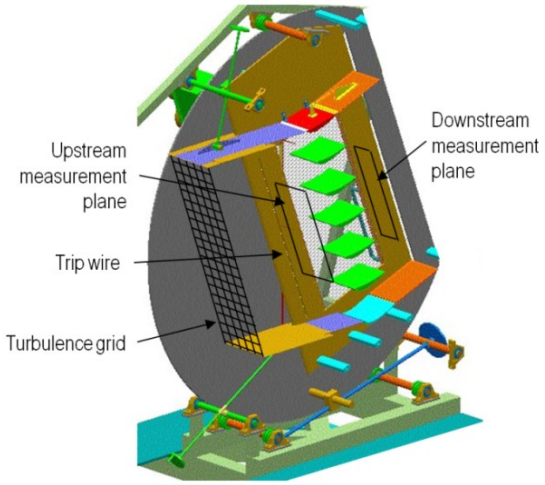

Fig. 1. Test Section of the Experimental Facility.

3 Measurement Procedure

Two traversing systems are used, one upstream and one downstream of the test section. The upstream traversing system is used for evaluating the quality of the incoming flow-field and to measure the incoming boundary condition. The downstream traversing system is used for investigating the downstream outflow properties. Both traversing systems are controlled by stepper motors. The positioning resolution is 1.6 μm for the downstream plane and 3 μm for the upstream plane. The upstream traversing system is moved in the (y, z) plane whereas the downstream one can be manoeuvred in the x direction also. Typical measurement planes are shown in Fig. 1.

Multihole pressure probes are used to measure the 3 velocity components and pressure in the flow. A 5-hole pressure probe is used at the upstream side whereas a 7-hole probe is used for the measurements at the downstream section. The probes were manufactured at

Chalmers. The diameter of the five-hole probe head is 3.5 mm with individual distances between the holes of 1 mm, and the tip half-cone angle of 45 degrees. The diameter of the seven-hole probe head is 2 mm with individual distances between the holes of 0.5 mm, and the tip half-cone angle of 30 degrees. The probes were calibrated at velocity of 20 m/s. The five-hole probe is calibrated for flow angles between 0 and 20 degrees, and the seven-hole probe for angles between 0 and 72 degrees.

The flow pressures were monitored by a 16-channel PSI 9116 digital pressure scanner (Pressure System Inc.) which has a measuring range of ±2500 Pa. The accuracy of the scanner in the measurement range of current experiment (±250 Pa) is ±2 Pa as validated by a calibration against a Furness Control PPC500 calibrator. The scanner performs channel scan at a fixed frequency of 500 Hz. During a typical measurement 1000 data samples were taken for each channel and the mean pressures were recorded. The sampling settings resulted in 0.8% statistical uncertainty of the mean with 99% confidence in regions with the highest fluctuations of pressure (10%). The absolute measurement uncertainty obtained for the pressure coefficient C_p is estimated around 0.01 and for the loss coefficient K_L around 0.001.

To monitor the pressure upstream of the suction system a Pitot tube is placed after the contraction but upstream of the suction slots. The static pressure taps on both end-walls at different pitch positions are placed to allow the possibility of measuring the uniformity of the inlet static pressure and to adjust the suction.

As the test rig has very good symmetry, the outlet measurements were taken over a half of the span one pitch length over the central blade. Spatial resolution of 2 mm (1% of span) in y and z-directions was used and over 4000 spatial points were measured in each plane. To avoid the wall proximity effects the measurements were always performed farther than two probe head sizes from the wall. A correction for the spatial velocity gradient effects was applied as described in [5].

Probe positioning and data acquisition were fully automated and controlled by a PC with NI LabVIEW software. Post processing of the experimental data was performed in Matlab (MathWorks Inc).

4 Experimental Geometries

The OGV geometry used for these investigations was developed at Chalmers as a demonstrator for OGV validation cases. The OGV consists of a 2D profile section which is extended in the span direction. The vane axial chord is 220 mm and the span is 200 mm. The design requirement for this vane is to turn the incoming flow with an inlet flow angle of 30 degrees to an axial outflow. The off-design requirements are ±10 degrees incidence without a mid-span separation.

A surface non-conformance was specially designed to simulate a generic welding trace. Figure 2 shows the vane with the welding trace. The height of the weld is 2.5 mm, and the width is 12 mm. The welding trace is two-dimensional and protruding through full blade span. The streamwise position of the weld on the vane is denoted as x_b.

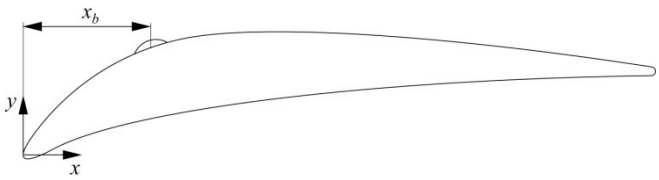

Fig. 2. Geometry Definition for the Non-conformance.

5 Preliminary Studies

The sensitivity of the flow in the cascade to 2D surface modifications of chosen type was studied parametrically by placing a 2D weld non-conformance at different locations on the vane. Results of the preliminary study were presented in paper [6] and this study was performed without establishing the flow periodicity in the cascade. A single welding trace was consecutively placed on the mid-vane of the cascade on the pressure side and on the suction side. Pressure distribution on the vane for different welding trace positions was monitored. From this study it was concluded that the pressure side of the vane is virtually non-sensitive to the surface modifications and

only minor load changes were observed for welds placed near the pressure side peak or near the trailing edge. However, for the welds placed on the pressure side the integral load change was substantially small, of order of 1%. The suction side of the vane revealed much larger flow sensitivity to surface modifications. For the weld locations around the suction peak, at x/C=0.1–0.4, the vane load was altered significantly, and the largest variation of the pressure coefficient was observed for weld positioned at x/C=0.2. From the preliminary study it was concluded that the most "dangerous" are locations of the welding trace around the suction side peak. Since the flow reveals the highest receptivity for the non-conformances located around the suction peak, in currents study experiments were performed for weld placements on the vane suction side around x/C=0.2.

An idea about the flow modification caused by non-conformances can be obtained from results of Figure 3, which shows data from numerical study [7]. As these results demonstrate, the welds placed around the suction side peak cause the separation of the boundary layer on the vane. The size of the separation zone is varying depending on the weld location. The worst case is realized for the weld location at x/C=0.2, and a massive stall is generated in this case. Obviously, this flow situation is undesirable for OGV and must be avoided.

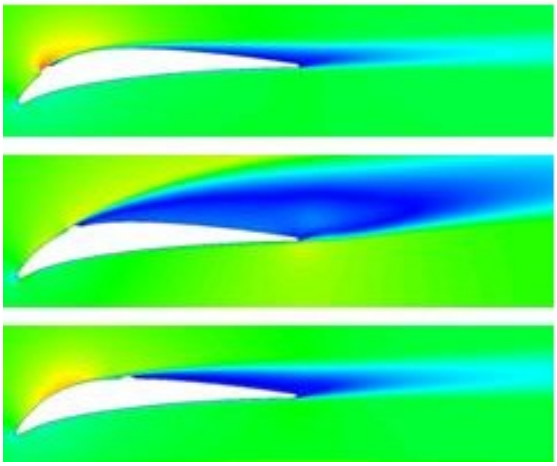

Fig. 3. Results of CFD Simulations [7] for Welding Traces at x/C=0.1, 0.2, 0.4 (From Top to Bottom). Contours of Velocity Magnitude from Calculations using k – ω SST Model.

It can be noted that the numerical simulations revealed large discrepancies between results obtained by different turbulent models in predicting the flow separation due to welds and the validation of the numerical results was main motivation for performing current experimental studies.

6 Experimental Results

Figures 4-5 show distribution of the pressure coefficient on vane for different weld placements. Figure 4 shows results for welding traces located upstream of the suction side peak at x/C=0.015–0.15 and Fig. 5 shows data for welding traces located at the suction side peak and farther downstream, at x/C=0.2–0.4. Position 0.2 is where the suction peak is located. Clean case data are shown for comparison in both figures. The pressure coefficient C_p is defined as:

$$C_p = P / q_{in,mwa} \qquad (1)$$

Where P is the pressure at a point on the vane surface, and $q_{in,mwa}$ is the mass-weighted average dynamic pressure at the inlet.

In current experiments the surface modifications were applied periodically, i.e. the welds were placed on three central vanes of the cascade and the flow was adjusted for periodicity.

Comparison of Fig. 5-6 shows that the influence on the flow of the welding trace in the area of the favourable pressure gradient (Fig. 5) is significantly less pronounced than in the area of adverse pressure gradient (Fig. 6). The effect from the welding trace very close to the vane leading edge is negligible (x/C=0.015) and does not alter the overall lift of the vane. Very thin boundary layers and favourable pressure gradient result that the flow is attached near the leading edge so that the effect of putting a perturbation whose size is very small compared to the size of the vane is very less. From Fig. 6 it follows that for the weld position at x/C=0.2, in the suction side peak, a drastic change of pressure distribution on the vane occurs. In this point a changeover of the pressure gradient takes place and the flow streamlines have the

largest curvature. As a result, placement of the welding trace creates a massive flow stall which can be seen as an area of constant pressure occurring downstream of x/C=0.3. Presence of this separating region creates losses and causing decrease of the de-swirling performance of the vane. One can also observe that for welding trace positions moving more towards the trailing edge the C_p plots start to resemble the plot for the clean case and the flow separation disappears. One can expect that the attached flow does not lead to rising losses. One can also notice that the separation margin is very sharp for current weld geometry and this fact explains observed earlier difficulties in prediction of the flow using turbulence modelling.

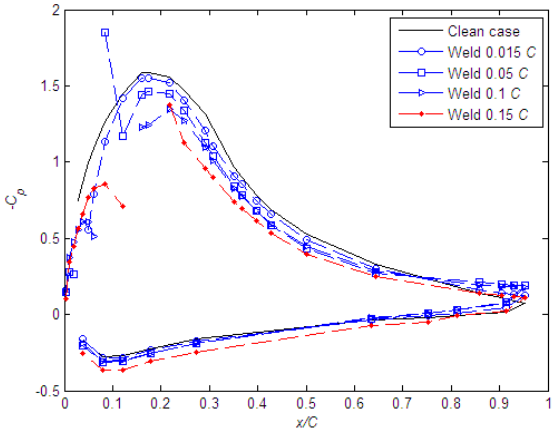

Fig. 4. Pressure Coefficient on Vane for Welding Traces Located Upstream of Suction Side Peak at x/C=0.015–0.15 in Comparison to Clean Case.

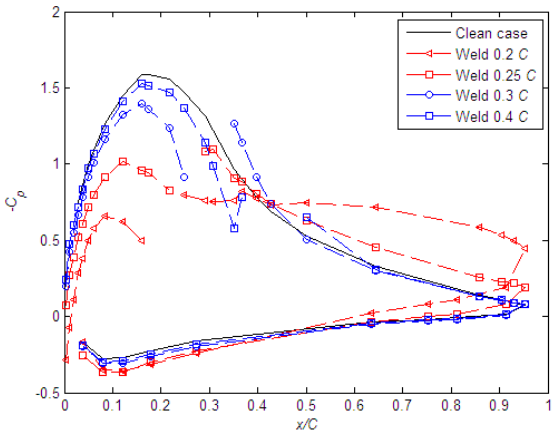

Fig. 5. Pressure Coefficient on Vane for Welding Traces Located at Suction Side Peak and Downstream, at x/C=0.2–0.4, in Comparison to Clean Case.

In Fig. 6-7 data for the downstream pressure loss in the wake at the vane symmetry plane are presented. The pressure loss coefficient is defined as follows:

$$\xi=(P_{tot,ref}-P_{tot})/q_{in,mwa} \qquad (2)$$

Where $P_{tot,ref}$ is the reference total pressure, which is the total pressure in the cascade freestream, P_t is the local total pressure at the outlet, and $q_{in,mwa}$ is the mass-weighted average dynamic pressure at the inlet.

Figure 6 shows the pressure losses for welding traces located upstream of the suction side peak at x/C=0.015–0.15 and Fig. 7 shows data for welding traces located at the suction side peak and farther downstream, at x/C=0.2–0.4. Clean case data are shown for comparison in both figures. One can notice that for the clean case the wakes have the smallest size due to thin boundary layer on the vane suction side. As the welding trace is added and move closer to the suction peak the wake size becomes bigger and losses increased. Noticeable that the losses are largest for position x/C=0.05 where a local loss maximum is attained. Position x/C=0.15 reveals very characteristic spikes which are due to very unstable behaviour of the flow for this weld position. This point seems to lie exactly on the edge of a big separation as observed for further location, x/C=0.15 and due to this any minor changes in the cascade blockage were causing changes in the flow.

Figure 7 shows the biggest wake size for the welding trace at x/C=0.2 and the wake becomes thinner as the welding traces are positioned closer to the vane trailing edge. From position x/C=0.3 the wake size is virtually constant as can be seen from comparison with position x/C=0.4 and the wake width is about double of that in clean case. One can assume that the wake size in the latter cases is caused by increased boundary layer thickness and no flow separation is triggered. The flow separation however occurs for positions x/C=0.2 and x/C=0.25. One can notice again the very sharp separation margin which follows from the fact that the separation is suppressed by moving welding trace only 0.05C downstream.

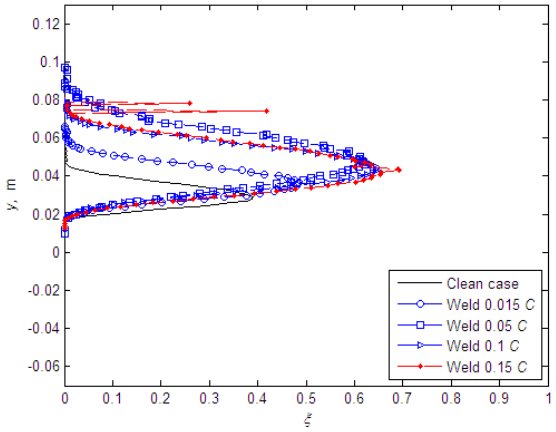

Fig. 6. Downstream Pressure Loss for Welding Traces Located Upstream of Suction Side Peak at x/C=0.015–0.15 in Comparison to Clean Case.

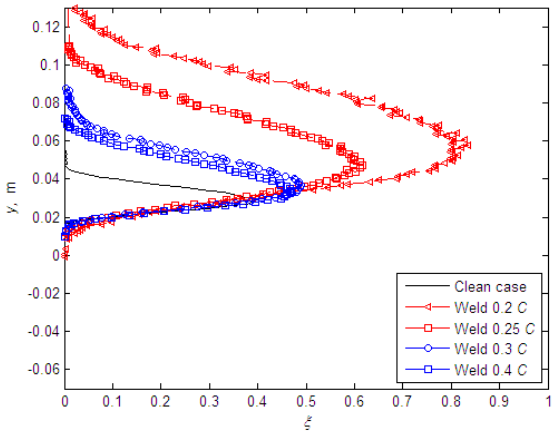

Fig. 7. Downstream Pressure Loss for Welding Traces Located at Suction Side Peak and Downstream, at x/C=0.2–0.4, in Comparison to Clean Case.

The main aerodynamic function of the OGV is to de-swirl the flow from the last low-pressure turbine rotor into an axial outflow which means that ideally the outflow angle from OGV cascade should be 0 deg. To study the weld effect on the OGV flow turning performance the outflow angles were compared for different cases in Fig. 8-9. As expected, for the cases with the flow separation the flow angle was altered the most. The de-swirling performance of the cascade is however characterized by the integral flow angle which will be discussed further. One can notice that for the test case x/C=0.20 the outflow angles are varying from −10 deg to +10 deg as compared to ±2 deg for clean case. The largest flow angle variation for the welding traces located upstream of the suction side peak can be observed for the case of x/C=0.05.

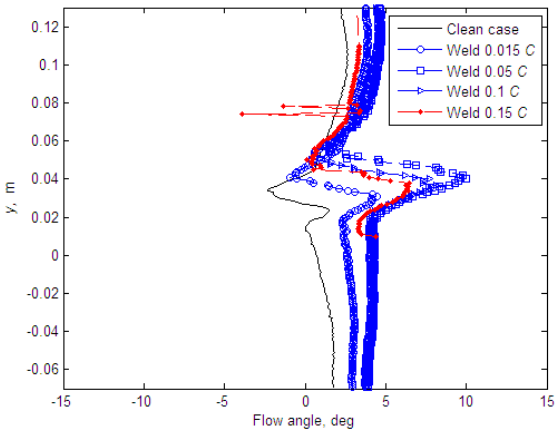

Fig. 8. Downstream Flow Angle Distributions for Welding Traces Located Upstream of Suction Side Peak at x/C=0.015–0.15 in Comparison to Clean Case.

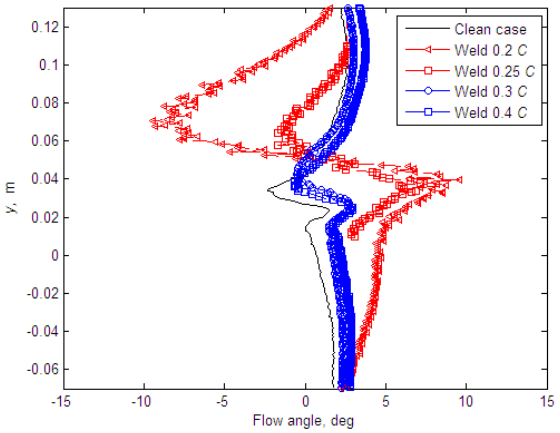

Fig. 9. Downstream Flow Angle Distributions for Welding Traces Located at Suction Side Peak and Downstream, at x/C=0.2–0.4, in Comparison to Clean Case.

The cross-flow planes obtained at the cascade outlet are shown in Fig. 10. This figure shows data for different weld positions and for the clean case. Only a half of the blade span is shown, and the cascade sidewall is located at z=-0.1 while the symmetry plane is at z=0. These diagrams show contour plots of the normalized total pressure. A detailed analysis of the secondary flow field for baseline configuration of the cascade was performed earlier, see ref. [3]. In particular, a boundary layer is developed on the cascade sidewall, and an interaction with the boundary layer from the blade suction side results in the maximum losses

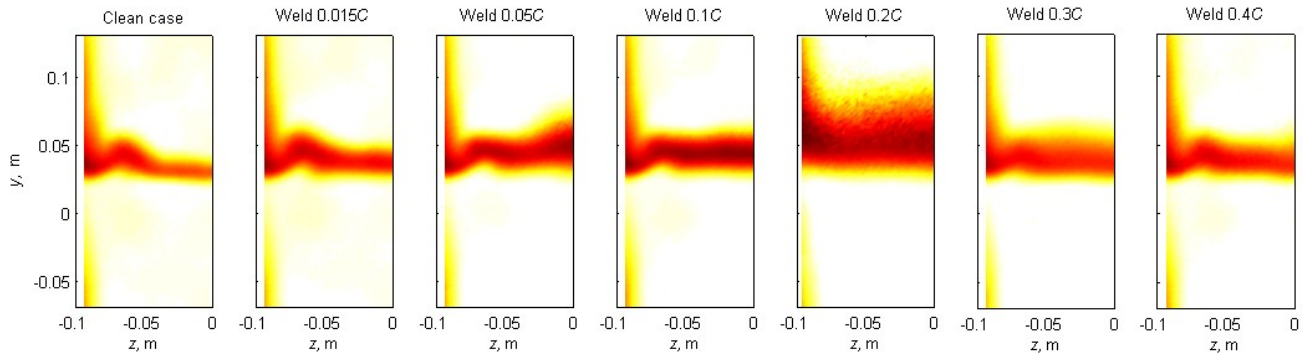

Fig. 10. Normalized Total Pressure Downstream of the Cascade Mid-Vane for Different Welding Trace Locations and for the Clean Case.

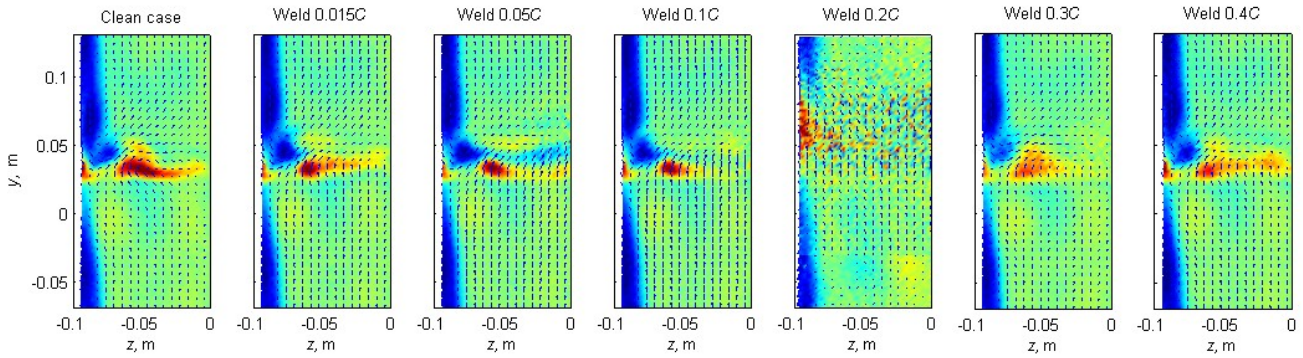

Fig. 11. Streamwise vorticity. Downstream of the Cascade Mid-Vane for Different Welding Trace Locations and for the Clean Case. Arrows Show Crossflow Velocity Components.

of pressure in the corner between the sidewall and the blade suction side. The increased loss is a result of the action of the secondary flow in the cascade and created suction side vortex, see [3] for more details. From the analysis of the wake planes for the cascade with non-conformances it can be noticed that the most pronounced change of the total pressure loss at the vane mid-span occurs for the weld positions at x/C=0.05 and 0.2 as was highlighted before. The noticeable wake increase in these two cases indicates that the flow separation is present. Form analysis of data in Fig. 10 it can be noted that case of weld located at x/C=0.05 is special as compared to other cases. For this case the wake shape becomes noticeably three-dimensional with substantially increased loss at the mid-span. For other cases shown in Fig. 10 except x/C=0.05 the wakes are essentially two-dimensional for at least 1/2 of the vane span. One can clearly see that the loss increase in all cases occurs due to increased profile loss, which is the loss in the mid-span. The losses due to the sidewall boundary layers and within the corner region are virtually not changed. Moreover, for all cases except the stalled case, x/C=0.2, the pressure losses are constant between z=–0.1 and z=–0.06. This fact is remarkable since for the off-design conditions of the increased inlet flow angle the losses are increasing approximately uniformly across the span [3]. In current cases the situation is different and the secondary loss remains constant close to the sidewall for all cases except x/C=0.2.

The streamwise vorticity is shown in Fig. 11 and provides further quantitative information on the modifications of the flow topology due to the welds. As known the secondary flows are linked to the streamwise vorticity. As Fig. 11 demonstrates the streamwise vorticity in the

passage is practically unaffected by the welds, with exception for the case x/C=0.2. For the latter case the generated massive two-dimensional stall is influencing the three-dimensional vortical structures and the sidewall boundary layers. It can be summarized that the flow modification due to welds is two-dimensional for all cases and the three-dimensionality only have certain significance for case x/C=0.05.

The summary of results for all welding traces is presented in Fig. 12. The integrated mass-averaged profile losses from experiments are compared to results of numerical study [7]. In work [7] 2D calculations were performed using two different turbulence models, $k-\omega$ SST and $k-\varepsilon$ realizable. In Fig. 12 also the loss from the baseline case is shown. It can be seen that as compared to the baseline case the experimental losses increase about ten times for the weld position at x/C=0.2 and about 2-5 times for other positions. From this figure it is also seen that the separation margin predicted by the $k-\omega$ SST model is delayed by approximately 0.05C, i.e. one can notice that the position x/C=0.3 in the $k-\omega$ SST predictions corresponds to the experimental position x/C=0.25. For the cases of welds between x/C=0 and 0.15 the 3D effects probably play an important role and 3D calculations are necessary. However, since the profile loss contributes to about 1/3 of the total passage loss, the predictions by the $k-\omega$ SST model can be considered reasonably good even under conditions of a 2D approximation. In the case of weld at x/C=0.1 the under-prediction of the loss by the turbulent models is very interesting to investigate in more detail. It is unclear which phenomena lead to the under-predicted loss in this case, the favourable pressure gradient, 3D effects, or the laminar-turbulent transition. The $k-\varepsilon$ realizable calculations show misleading results for this geometry and missing the flow separation occurring for weld at x/C=0.2. In the zone of the favourable pressure gradient the $k-\varepsilon$ realizable model demonstrates very similar predictions as the $k-\omega$ SST, and reveals a peak of loss at x/C=0.05. This means that in the favourable pressure gradient both turbulence models seem to perform equally.

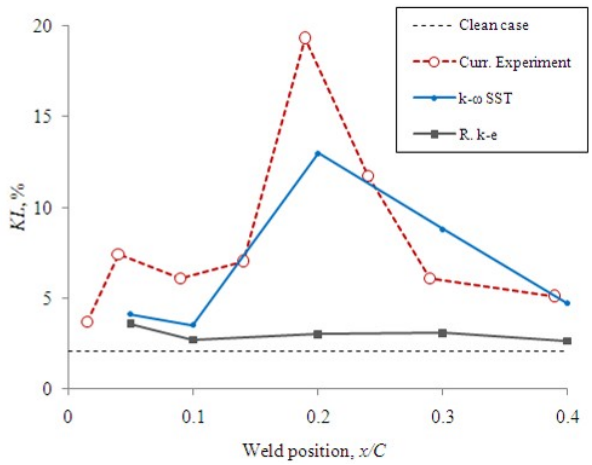

Fig. 12. Integral Total Pressure Loss at the Symmetry Plane in Comparison to CFD Data [7].

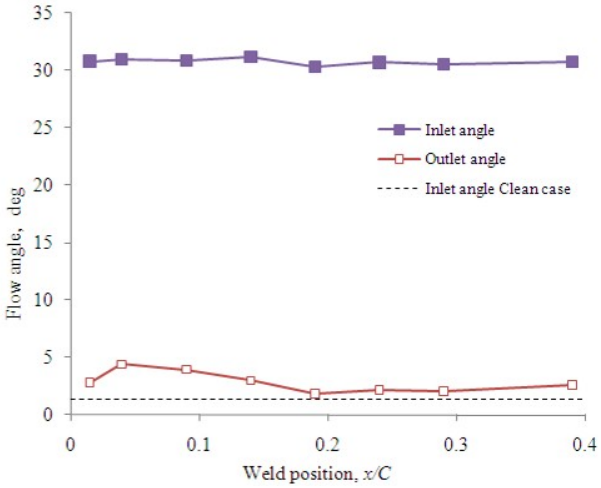

Fig. 13. Integral Inlet Flow Angle and Integral Outlet Flow Angle at the Symmetry Plane.

Results for integrated flow angles are depicted in Fig. 13. As can be noticed the integral flow angles are not affected significantly by the welds and the largest variation is seen for the welds located upstream of the suction peak. As was discussed before the largest variation of the angle amplitude is attained for case x/C=0.2.

7 Conclusions

Experimental results for a highly loaded LPT/OGV cascade equipped with simulated surface geometry variations are presented. The influence of surface nonconformance in the form of a two-dimensional welding trace is investigated. Results for load distributions, losses, outlet flow angles and the evolution of the secondary flow-field are monitored and analyzed. This study shows in which way this type of surface geometry variation and it position affect the OGV performance. Noticeable that even relatively large surface defects as were investigated may have insignificant role for the OGV performance if they are located at specific locations on the vane surface. On the other hand there is another range of locations on the OGV surface in the region of the suction side peak where the surface deteriorations influence the aerodynamical properties considerably. A significant increase of the pressure loss occurs when the flow separation is triggered. This means that positions on the OGV surface and corresponding surface treatment can be identified providing that design and repair rules for the OGVs can be developed.

References

[1] Wisler, D:C., The technical and economic relevance of understanding blade row interaction effects in turbomachinery, in *Blade row interference effects in axial turbomachinery stages*, Von Karman Institute for Fluid Dynamics, LS 1998-02, 1998.

[2] Hjärne, J., Larsson, J. and Löfdahl, L., Design of a modern test-facility for LPT/OGV flows, *ASME paper* GT2003-38083, 2003.

[3] Hjärne, J., Chernoray, V., Larsson, J., Löfdahl, L., Experimental analysis of the flow-field in a state of the art linear cascade with boundary-layer suction, *ASME paper* GT2005-68399, 2005.

[4] Hjärne J., Turbine outlet guide vane flows, *PhD thesis*, Chalmers University of Technology, Göteborg, Sweden, 2007.

[5] Chernoray V., Hjärne, J., Improving the accuracy of multihole probe measurements in velocity gradients, *ASME paper* GT2008-50492, 2008.

[6] Chernoray V., Larsson, J., Ore S., Effect of geometry deviations on the aerodynamic performance of an outlet guide vane cascade, *ASME paper* GT2010-22923, 2010.

[7] Alonso, R., Non conformance effects on outlet guide vanes, *Master thesis*, Chalmers University of Technology, Göteborg, 2009.

Contact Author Email Address

valery.chernoray@chalmers.se

Copyright Statement